Soil Moisture Sensor Measurement and Vegetation-Soil-Water Related Indices – A Case Study in Mango Plantation, Nakhorn Ratchasima Province, Thailand

Pensuk Tibkaew, A.,[1] **Miyai, J.,**[2] **Buakhao, W.**[3] **and Phonekeo, V.**[4*]

[1]Department of Geography, Faculty of Social Sciences, Kasetsart University, 50 Ngamwongwan Rd., Ladyao, Chatuchak 10900, Bangkok, Thailand, E-mail: anisara.pensuk@gmail.com

[2]Civil Engineering Specialist, Office of Engineering for Land Development, Land Development Department, Ministry of Agriculture and Cooperatives, 2003/61 Phaholyothin Road, Ladyao, Chatuchak, Bangkok, Thailand, 10900, E-mail: nnoomm@hotmail.com

[3]Engineering and Technology Group, Office of Engineering for Land Development, Land Development Department, Ministry of Agriculture and Cooperatives, 2003/61 Phaholyothin Road, Ladyao, Chatuchak, Bangkok, 10900, Thailand, E-mail: ch_panya@hotmail.com

[4]P.O. Box 65, Khlong Luang Post Office, Pathumthani 12120, Thailand, E-mail: vivarad@gmail.com

[*]*Corresponding Author*

DOI: https://doi.org/10.52939/ijg.v18i2.2155

Abstract

This study conducted the soil moisture estimation using remote sensing data and ground soil moisture sensors in the mango plantation. The applied methodology is the spatial and statistical analysis to determine the relationship between the measured soil moisture using ground sensors and the remote sensing indices generated from Sentinel-2A satellite images. The sensors measured the soil moisture ground data from Nov. 2019 to Feb. 2020. However, we used only the data on seven dates. This is because the cloud-free satellite images are available only on these dates to generate the remote sensing indices. The used indices are NDVI, Normalized Water Moisture Index (NDWI) for vegetation water content monitoring, Normalized Soil Moisture Index (NSMI) for data visualization and analysis. In the implementation, we first visualized the soil moisture trend compared with the remote sensing indices value at the image pixels of sensor location on each observation day. Next, we statistically analyzed the spatial data to establish the relationship between the soil moisture from all the ground sensors and the remote sensing indices. However, the output R^2 is very low; then, it brings us to have an idea to apply in-depth analysis based on the ground sensor performance. This method shows an interesting result. We found that only the NDWI for monitoring vegetation water content has a similar trend with the soil moisture. Secondly, we performed the linear regression correlation between soil moisture and remote sensing indices values of each sensor as time-series analysis. The result show that the correlation between soil moisture and NDWI, NSMI and NDVI are classified into 3 groups, which are $0.7 < R^2 < 0.9$, $0.6 < R^2 < 0.7$, and $R^2 < 0.5$, where their corresponding p-value ranges are $0.001 <$ p-value < 0.02, $0.01 <$ p-value < 0.03, and $0.08 <$ p-value < 0.9, respectively. Lastly, we investigated the reason that causes the very high correlation between the soil moisture value of the first group of sensors and NDWI and NSMI. The result shows that these sensors are in a sparse vegetation cover area, where NDVI ≤ 0.3. Therefore, according to this, we can conclude that remote sensing indices NDWI and NSMI can be applied for soil moisture estimation in a sparsely vegetated study area, where the NDVI value should be less than or equal to 0.3.

1. Introduction

Soil moisture is an important variable for natural disasters and environmental applications. In agriculture, it directly impacts plant health, drought monitoring, and water resources management. Because of this, a research project to implement soil moisture measurement using a sensor measurement system in the sample agricultural fields is necessary. Therefore, soil measurement sensors network as the Internet of Things (IoT) for agriculture is applied to the mango plantation.

This project is a collaboration between Kasetsart University, Walailak University, Valaya Alongkorn Rajabhat University, and Office of Engineering for Land Development (OELD) under the Land Development Department of Thailand.The sensors network measures the soil moisture in near real-time and is controlled online. The measured data are transmitted online in the defined interval to the cloud web server. These data archives in the database operate in the mobile application 'Agri-Map'. The project provides a low-cost measurement system, affordable for the farmers. However, using ground sensors to measure soil moisture can be done only in a limited area. It is not possible to establish an extensive sensor measurement system to a large extent due to budget and maintenance costs. Therefore, the only efficient way to monitor the soil moisture status in sizeable agricultural land is to apply remote sensing, and GIS. Various research involved remote sensing technology for soil moisture estimation using different techniques were conducted.

Ahmad et al., (2011) summarized various remote sensing methods for soil-moisture estimation. They have pointed out that many research papers have introduced different methods to retrieve soil-moisture information from different remote sensing data types, such as optical data or radar data. They evaluated the most potential methods for retrieving soil-moisture information of bare soil and vegetation-covered soil. They overviewed soil-moisture retrieval methods using different remote sensing data, including active or passive. They have compared the results of the methods, including the advantages and limitations of each method. The comparison shows that a combination of both active and passive sensing methods provides reliable results. Petropoulos et al., (2015) explained that all electromagnetic spectrum regions could measure soil moisture and various techniques to some level or different. They provided a whole scenario of the applications made during the last 20 years to estimate surface soil moisture using satellite imagery, mainly focusing on retrievals from microwave sensors. In this research work, they considered the new techniques developed by combining optical and thermal infrared remote sensing, active and passive microwave. Ray et al., (2017) conducted a study to evaluate four significant soil moisture (SM) products derived from satellite imagery over the state of Texas, which are related to different remote sensing systems. The systems are Advanced Microwave Scanning Radiometer—Earth Observing System (AMSR-E), the Soil Moisture Ocean Salinity system (SMOS), AMSR2, and the Soil Moisture Active Passive system (SMAP). This study shows that sensor accuracy and the applied algorithms used in the data processing process influence the generated SM data quality. The soil moisture measurements are considered reasonable and effectively used for different applications, including flood forecasting and drought prediction. Filion et al., (2015) applied microwave and optical remote sensing data to generate reliable soil moisture maps to support water management and agricultural practice in Mediterranean regions, particularly during dry seasons. The research is based on field surveys in the period from 2005 to 2009 in Sardinia, Italy. The result is an empirical model for estimating bare soil moisture, with a coefficient of determination (R^2) of 0.85. They also used Landsat TM5 satellite imagery for soil moisture estimation using the temperature and vegetation index relationship, which produced the best linear relationship with an R^2 of 0.81. Two empirical models using C-band SAR data for assessment of surface moisture show the R^2 of 0.76. A downscale model on soil moisture estimation is shown in research by Park et al., (2017) using remote sensing physical variables using the Global Land Data Assimilation System (GLDAS) soil moisture. This data used as a reference dataset for the East Asian region based on optimizing a modified regression tree. They used six variables from microwave, optical remote sensing, and digital elevation models. Land Surface Temperature (LST), Normalized Difference Vegetation Index (NDVI), and land cover use as input variables. The study shows a reliable result, which is daily high-resolution soil moisture data from various satellite sources. Babaeian et al.,, (2019) has developed the OPtical TRApezoid Model (OPTRAM) used for watershed-scale soil moisture estimation based on shortwave infrared (SWIR) transformed reflectance (TRSWIR) and the normalized difference vegetation index (NDVI) from remote sensing data. Their research aimed to evaluate OPTRAM for field-scale precision agriculture applications using ultrahigh spatial resolution optical observations obtained with field robotic phenotyping scanners located in Maricopa, Arizona. Machine learning technique also was used in the research conducted by Torres-Rua et al., (2016). They have described in their study a new approach to estimate volumetric surface soil moisture by statistical analysis of different potential predictors that include vegetation indices and energy balance products generated from Landsat imagery and weather data.

This technique applied a statistical learning machine called a Relevance Vector Machine (RVM) to identify the potential predictions for soil moisture estimation utilizing stratified cross-validation and forward variable selection. Alexandridis et al., (2016) noted in their research that soil moisture is hard to estimate the soil moisture at the catchment scale and frequent periods, as is required by many hydrological, erosion, and flood simulation models. They described a methodology to estimate soil moisture using the satellite-derived evaporative fraction with soil and meteorology information. They also used a time series of MODIS satellite data to estimate soil moisture maps with eight days at a 250-m spatial resolution for three different catchment areas in Europe. The results show that the developed technique can estimate soil moisture maps at the studied scale, within the 250-m spatial resolution of eight days. The soil moisture estimation in coastal soils was conducted by Klemas et al., (2014) to understand the soil properties necessary for agriculture and maintaining natural environments, including wetlands. The authors analyzed the beach characteristics, which are soil moisture, grain size, and type. The new applied technology allowed microwave remote sensing to measure soil moisture globally in the top of few centimeters. The advantage of remote sensing can be used with the ground sensor measurement system, where the ground sensor can provide in-situ soil moisture data, then, the soil moisture estimated from satellite imagery can be validated using the in-situ data.

2. Scope of the Study

This research aims to establish the relationship between the measured in-situ data and the remote sensing indices. In this research, the scope is detailed as below:

- Since the selected study area of this collaboration project is not large, then the number of sensors for soil moisture measurement used in this research is limited.
- We have selected the remote sensing indices, NDVI, NDWI, and NSMI, obtained from the satellite images to be the leading indices to establish their relationship with the soil moisture data measured in the study area. These are the main variables of the study.
- The methodology used here is the straightforward statistical analysis to establish the relationship of the variables listed above. Consequently, the results obtained from the analysis provide different correlation levels of these variables.

3. Study Area

The study area is the experimental mango plantation plot locates in the Pakchong district of Nakhon Ratchasima Province, Northeastern Thailand, at 14.6783° N, 101.4176° E as shown in Figure 1.

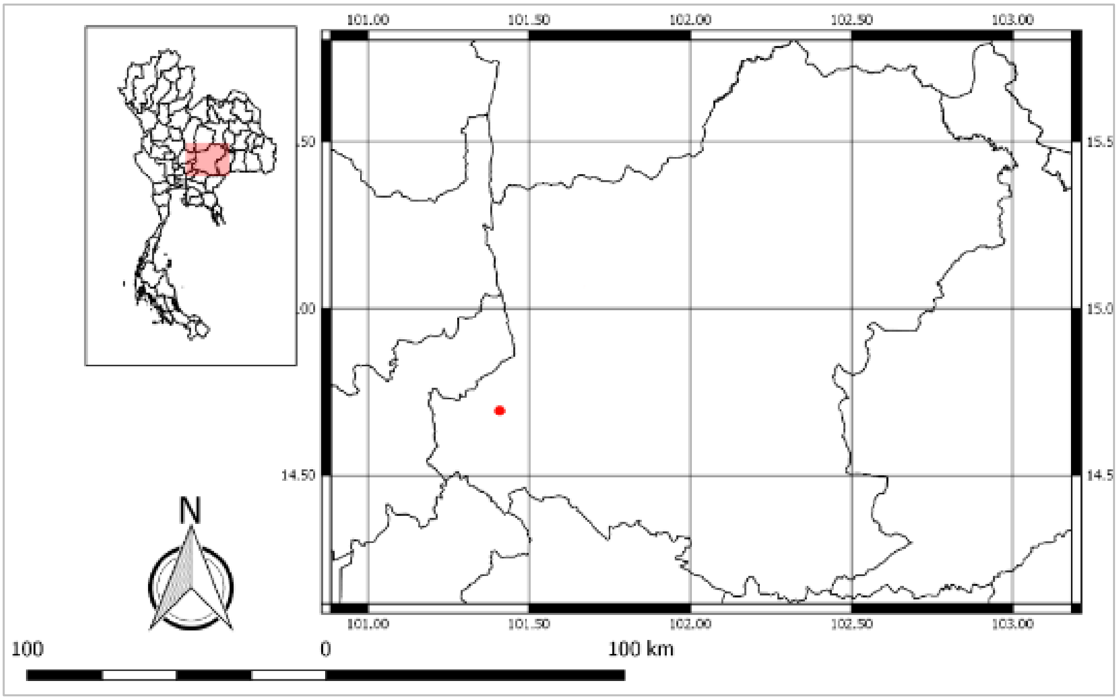

Figure 1: Map of Nakhorn Ratchasima province with the study area shown by a red dot

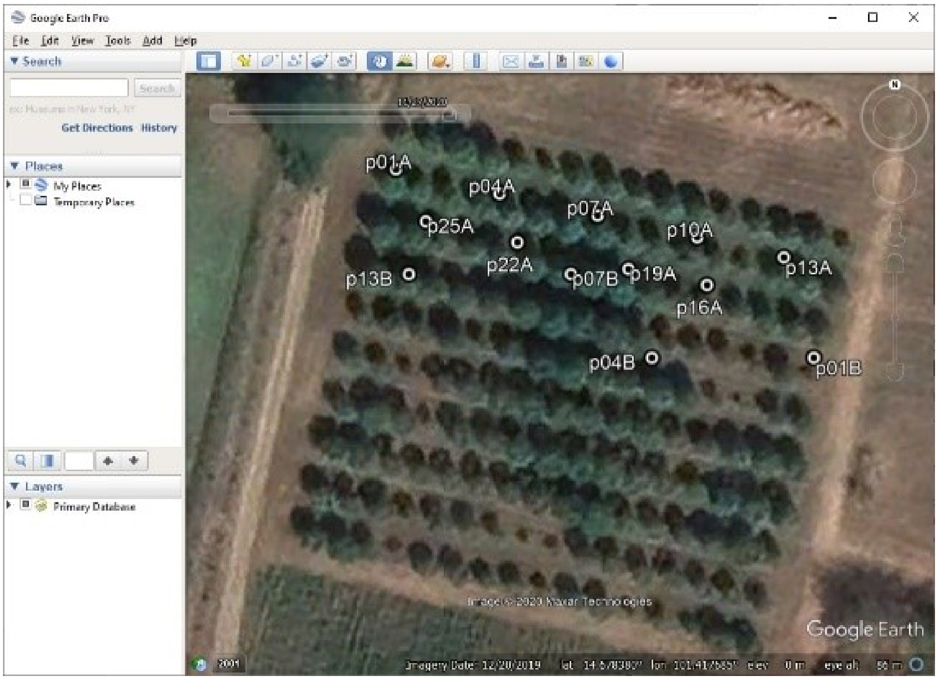

Figure 2: A very-high-resolution Satellite image from Google Earth dated Dec. 20, 2019 shows the study area and the soil moisture sensors with labeling numbers

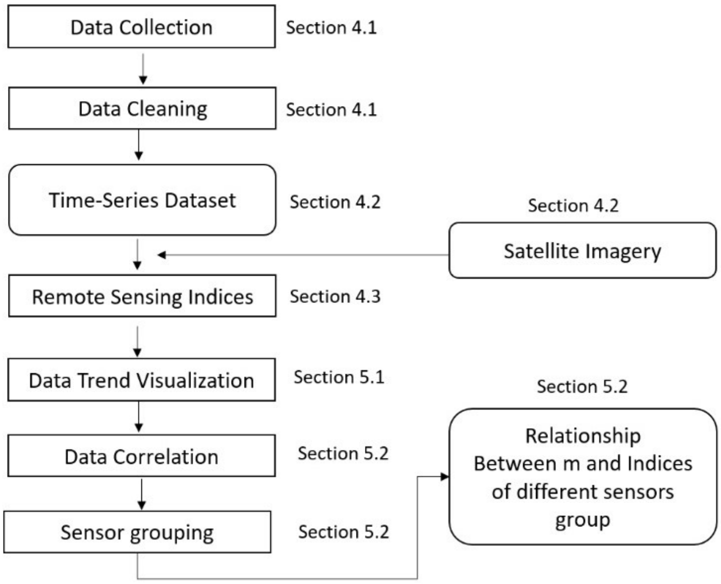

Figure 3: Flowchart of the methodology of the study

This plot belongs to the Land Development Research and Technology Transfer Center (LDRTTC) in the district. The plot's size is 55 m vertical by 64 m horizontal, as shown in Figure 2. However, the ground measurement sensors' distribution covers only about half of the plot, in the upper part. The characteristics of the study area in terms of soil properties: the soil is deep and well drainage, clayey, and clay loam texture. The land use here is mainly covered by maize fields but with some orchards.

4. Methodology and Data

The methodology in this study consisted of the following parts, which are illustrated in the flowchart below (Figure 3). The study started with the soil moisture data (denoted as *M*) collection from the sensors.

Then, the data cleaning was applied to select only the relevant parameters for the study and grouped them into daily soil moisture datasets (Section 4.1). Next, these datasets were compared with the remote sensing satellite imagery to establish a time-series of daily matching data pairs consists of *M* and satellite data for the same acquisition date and time (Section 4.2). Normalised Difference Vegetation Index (NDVI), Normalised Difference Water Index (NDWI) developed for vegetation water content monitoring (Gao, 1996), and Normalized Soil Moisture Index (NSMI) images were generated for the selected time-series dataset (Section 4.3). Applying these datasets of *M* and its corresponding indices, the visualization of the trend for *M* comparing with the indices value in each matching daily dataset was carried out (Section 5.1). Next, the linear regression correlation between ***M*** and the indices for each sensor as a time-series analysis is performed (Section 5.2). The result brings us to the reason that causes different values R^2 of the relationship between m and NDWI and NSMI for the sensors in the study area. The details of the methodology's implementation are explained in sections 4.1-4.3, and the results are shown in sections 5.1-5.2.

4.1 Soil Moisture Sensor Measurement Data Collection

The soil moisture measurement system used in this research consists of 13 sensors divided into two groups as A and B. The Group A has 9 sensors, (with labels as 01A, 04A, 10A, 07A, 13A, 16A, 19A and 25A) and group B has 4 sensors (with labels of 01B, 04B, 07B, and 13B). All of the sensors were positioned in the depth of 10 cm below the soil surface. The letter 'p' in Figure 4 denoted the sensor as a point. The soil moisture value used in this study was the moisture of the soil at the depth of 10 cm below the soil surface. In order to learn about the accuracy of the sensors, the SM150T soil moisture sensor was used for calibration and it has dependable ± 3% soil moisture accuracy.

The spacing between the sensors is 6 m and 8 m in the diagonal and vertical direction. The sensors were positioned followed the mangos' canopy. The NDVI image below (Figure 4) generated using the Sentinel-2 data, acquired on December 18, 2019, to show the locations of the sensors comparing to the Sentinel-2 image pixels. Most of the sensors were locating in the different pixel except 04A and 22A which is located in the same pixel. In this case, the measured soil moisture of these two sensors during the observation period is nearly similar (0.15-0.18%), which the difference is very small, that is about 0.03%. Therefore, we can use the measured soil moisture from one of them.

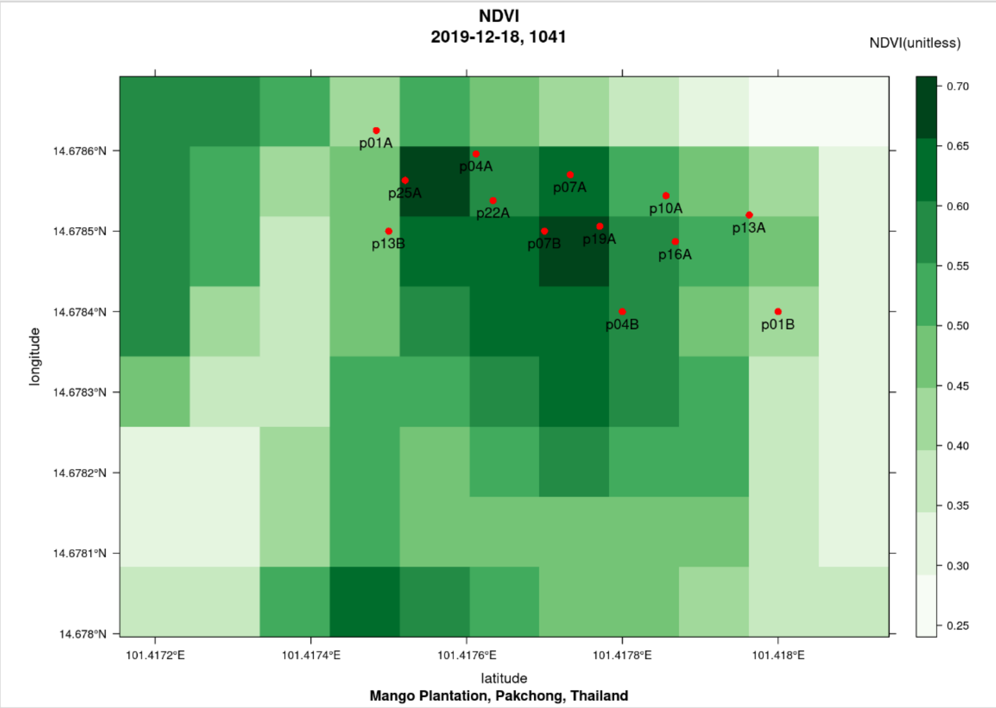

Figure 4: The locations of the sensors comparing to the Sentinel-2 image pixels

These sensors are connected to the controller box, consisting of an electric controller, data collector, and Internet connection box for data transferring to the data archiving system on the cloud. The sensors collect the soil moisture data from Nov. 07, 2019, to Feb. 04, 2020, in CSV format with different variables. The geographic coordinates of the sensors were shown in Table 1.

4.2 Sentinel-2 Satellite Imagery

Since the study area is approximately 3,500 m^2, which is not large, and we need precise details of the ground cover. Therefore, we selected the satellite imagery acquired by the Sentinel-2A and 2B. The Sentinel-2 mission belongs to the Copernicus program, which has been developed and operated by the European Space Agency (ESA) since June 2015. Both Sentinel-2A and 2B is a sun-synchronous-orbit satellite at the altitude of 786 km. These satellites have a similar primary sensor named Multispectral Instrument (MSI) that has 13 spectral bands ranging from visible, near-infrared (NIR), and shortwave infrared (SWIR), with three spatial resolutions of 10, 20, and 60 m. The field of view or image swath of 290 km. The revisit frequency of each satellite is 10 days, where the combination of their revisit is 5 days. The MSI instrument has a radiometric resolution of 12 bits per pixel, which allows the image to have a range of 0 to 4095 potential light intensity values or grey levels for the digital pixel value. The satellite images are freely available at the Sentinel Hub website (sentinel-hub.com). The Spectral bands for the Sentinel-2 sensors are shown here below in Table 2 (Wikipedia, 2021).

Table 1: Part of the soil moisture data after data cleaning with the total number of 15 sensors in group B

Device ID	Hum	Lng	Lat	Record Time	Record Time
1	28.10	101.4180	14.6784	2019-11-07	22:15:45
2	24.80	101.4180	14.6784	2019-11-07	22:15:45
3	16.70	101.4180	14.6784	2019-11-07	22:15:45
4	27.90	101.4178	14.6784	2019-11-07	22:15:45
5	27.50	101.4178	14.6784	2019-11-07	22:15:45
6	20.40	101.4178	14.6784	2019-11-07	22:15:45
7	8.80	101.4177	14.6785	2019-11-07	22:15:45
8	27.40	101.4177	14.6785	2019-11-07	22:15:45
9	18.90	101.4177	14.6785	2019-11-07	22:15:45
10	0.00	101.4176	14.6785	2019-11-07	22:15:45
11	25.50	101.4176	14.6785	2019-11-07	22:15:45
12	0.00	101.4176	14.6785	2019-11-07	22:15:45
13	22.50	101.4175	14.6785	2019-11-07	22:15:45
14	29.10	101.4175	14.6785	2019-11-07	22:15:45
15	30.70	101.4175	14.6785	2019-11-07	22:15:45

Table 2: List of 13 soil moisture sensors in groups A and B with their ID number and geographic coordinates in Longitude (Lon.) and Latitude (Lat.) used in this study

ID	Lon.	Lat.	ID	Lon.	Lat.
01A	101.4175	14.6786	22A	101.4176	14.6785
04A	101.4176	14.6786	25A	101.4175	14.6786
07A	101.4177	14.6786	01B	101.4180	14.6784
10A	101.4179	14.6785	04B	101.4178	14.6784
13A	101.4180	14.6785	07B	101.4177	14.6785
16A	101.4179	14.6785	13B	101.4175	14.6785
19A	101.4178	14.6785			

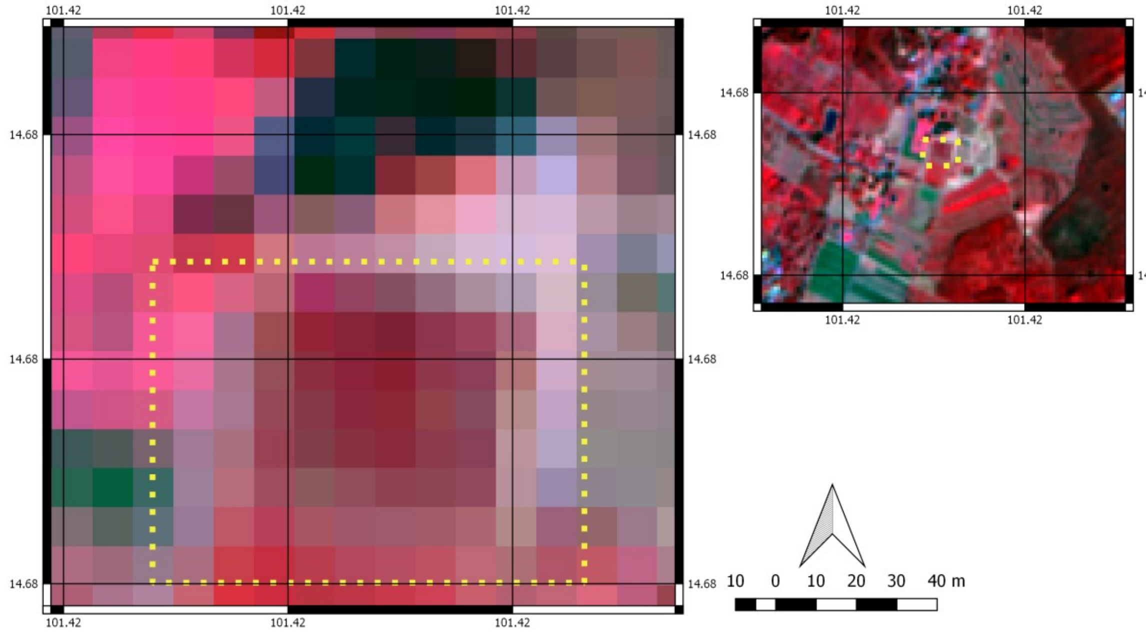

Figure 5: The study area (highlighted by yellow dash-line box) and surrounding, shown by Sentinel-2A image in the false-color composite based on bands 8,4,3 on the acquisition date of Dec. 13, 2019

Since the sensors collect soil moisture data from Nov. 07, 2019, to Feb. 04, 2020; however, the less-cloud Sentinel-2 image data in archiving at Sentinel Hub are available only for 7 dates, which are Nov. 08, 2019, Dec. 08, 2019, Dec. 13, 2019, Dec. 18, 2019, Jan. 27, 2020, and Feb. 01, 2020, at 03:40-03:42 GMT, which form our observation period of 7 dates. Figure 5 illustrates the Sentinel-2A image in false-color composite based on bands 8,4,3 covering the study area (highlighted by yellow dash-line box) and surrounding for the acquisition date of Dec. 13, 2019.

4.3 Remote Sensing Vegetation-Water-Soil Related Indices

The study area is covered by different sizes of tree crows and leaves densities that define the dense and sparse vegetation density. If we use only the soil moisture index images generated by satellite imagery, it would not be possible to have the soil moisture estimation on the ground surface. The dense vegetation blocks the satellite sensor visibility and can deviate the soil moisture estimation. Therefore, we applied remote sensing indices that are related to vegetation and water. The indices are the normalized difference vegetation index (NDVI), Normalized Difference Water Index (NDWI) (Gao 1996) for monitoring water content in vegetation leaves, and the Normalized Soil Moisture Index (NSMI). Since NSMI was used to find the correlation with NDVI generated from Sentinel-2 (Carmelo et al., 2019), we use it as the primary index together with NDWI. NDVI is used only as a supplementary index at the end of the study to describe the vegetation density in the area. The definition of these indices is shown by the following Equations (1) – (3) below:

$$\mathrm{NDVI} = \frac{\mathrm{NIR} - \mathrm{Red}}{\mathrm{NIR} + \mathrm{Red}}$$

Eqaution 1

$$\mathrm{NDWI} = \frac{\mathrm{NIR_n} - \mathrm{SWIR}}{\mathrm{NIR_n} + \mathrm{SWIR}}$$

Eqaution 2

$$\mathrm{NSMI} = \frac{\mathrm{SWIR_1} - \mathrm{SWIR_2}}{\mathrm{SWIR_1} + \mathrm{SWIR_2}}$$

Eqution 3

In equation (2) and equation (3), $\mathrm{NIR_n}$ is Narrow NIR (Band 8A), $\mathrm{SWIR_1}$ and $\mathrm{SWIR_2}$ is Shortwave infrared band of Band 11 and Band 12, respectively. Figure 6 shows an example of vegetation-water-content indices: NDVI, NDWI, and NSMI of the study area for the case of Dec. 13, 2019.

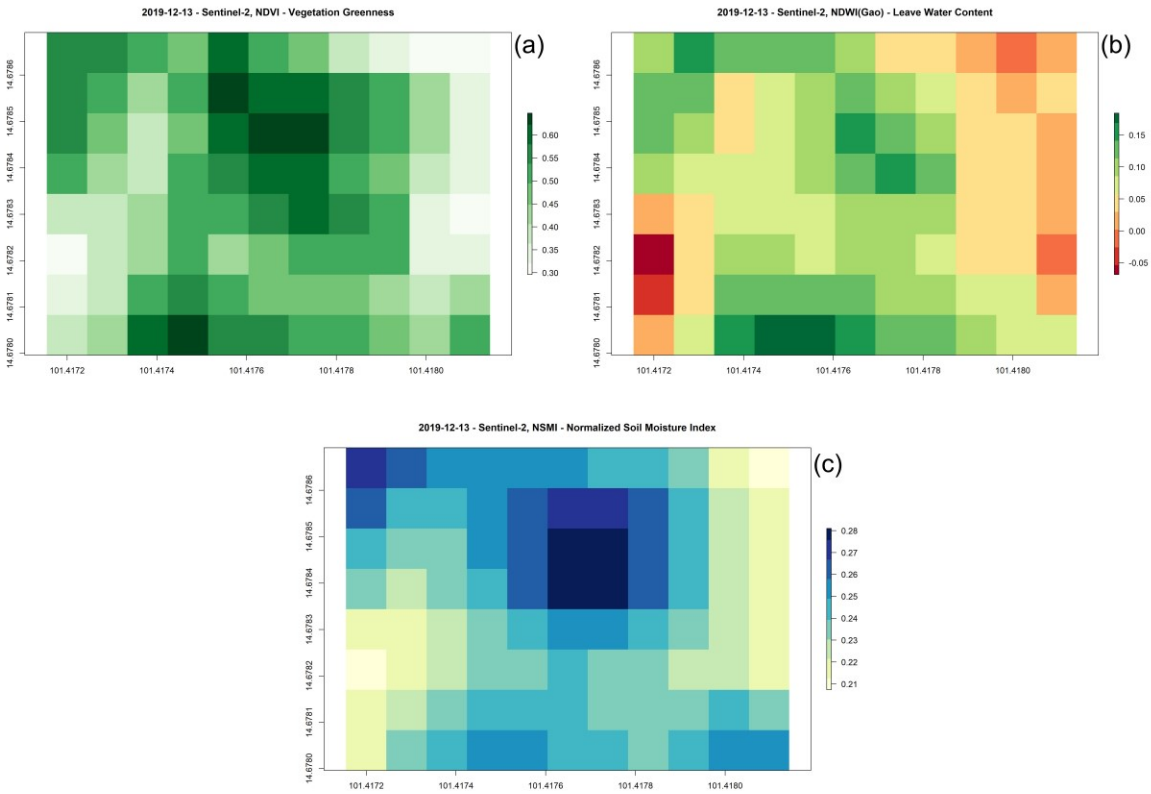

Figure 6: Examples of vegetation-water-content indices: (a) NDVI, (b) NDWI, and (c) NSMI of the study area for the case of Dec. 13, 2019

5. Results

5.1 Visualization and Comparison Trend of Measured Soil Moisture with Remote Sensing Indices

We denoted the soil moisture value, measured by the ground as *m*. The data analysis started with the visualization of the changing trend compared with the remote sensing indices value (NDWI and NSMI) in the observation period of 7 dates. Here, since the indices have the range of -1.0 to 1.0, we normalized the M value from its range 0-100% to 0.0-1.0 and denoted it as m to have consistency with the indices. Since the range of *m* and indices is normalized, we denoted this normalized value as *n*, and put it on the vertical axis of the graphs in Figures 7-13. In this part of the data analysis, we have removed sensor 07B, as described in Section 4.1 Therefore, there are only 12 sensors on the horizontal axis of the graph. The result shows that *m* and NDWI get along with each other for most of the dates as shown in Figures 7-13.

*5.2 Linear Regression Correlation between **Measured Soil Moisture** and Remote Sensing Indices Values*

Initially, the whole dataset of all 13 sensors during the observation period were used to analyze the relationship between the soil moisture data *m* collected by the sensors and their corresponding remote sensing indices. Then, in the sub-section 5.2.1, we will describe the relationship between the measured soil moisture with each of the remote sensing indices starting with NDWI and following with the description of the relationship between m and NSMI in next sub-section 5.2.2. After that, based on the finding in these two subsections, we group the sensors with very high, high and low correlation between m and NDWI and NSMI.

*5.2.1 Linear regression correlation between **measured soil moisture** and NDWI*

In the previous section, we have seen that the variables *m*, which is the measured soil moisture value and NDWI have similar trends for most observation dates.

This section analyzes the relationship and trends between these values of each sensor in a time series of all dates.

Table 3 shows an example of m value and corresponding remote sensing indices for each date of sensor 01A.

Table 3: Soil moisture and its corresponding remote sensing indices value of sensor 01A for each date

ACQ. Date	**ACQ. Time**	***m***	**NDWI**	**NSMI**	ID
Nov. 08, 2019	10:40	0.3060	0.2216	0.2672	01A
Dec. 03, 2019	10:41	0.2780	0.1597	0.2400	01A
Dec. 08, 2019	10:41	0.2710	0.1643	0.2391	01A
Dec. 13, 2019	10:41	0.2700	0.1208	0.2514	01A
Dec. 18, 2019	10:41	0.2720	0.1115	0.2445	01A
Jan. 27, 2020	10:42	0.2570	0.0861	0.1834	01A
Feb. 01, 2020	10:42	0.2530	0.0496	0.2072	01A

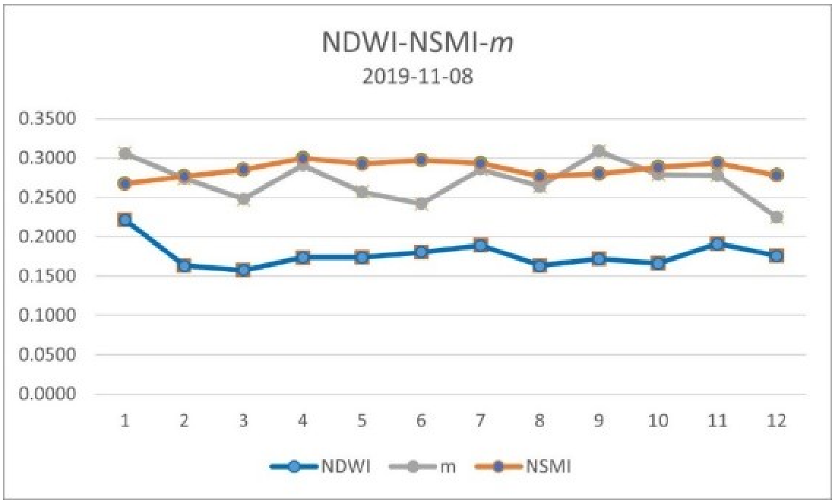

Figure 7: Comparison Trend of Measured Soil Moisture *m* with NDWI, and NSMI for the case of Nov. 08, 2019

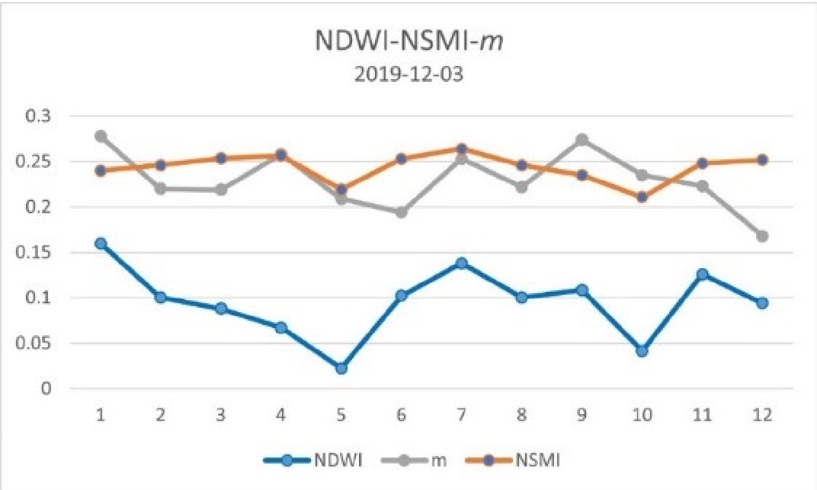

Figure 8: Comparison Trend of Measured Soil Moisture *m* with with NDWI, and NSMI for the case of Dec. 03, 2019

ISSN 2673-0014 (Online) / © Geoinformatics International

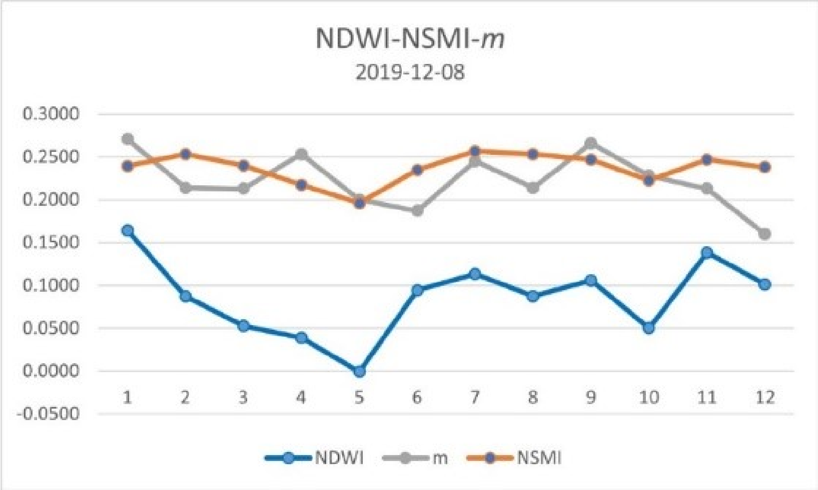

Figure 9: Comparison Trend of Measured Soil Moisture *m* with NDWI, and NSMI for the case of Dec. 08, 2019

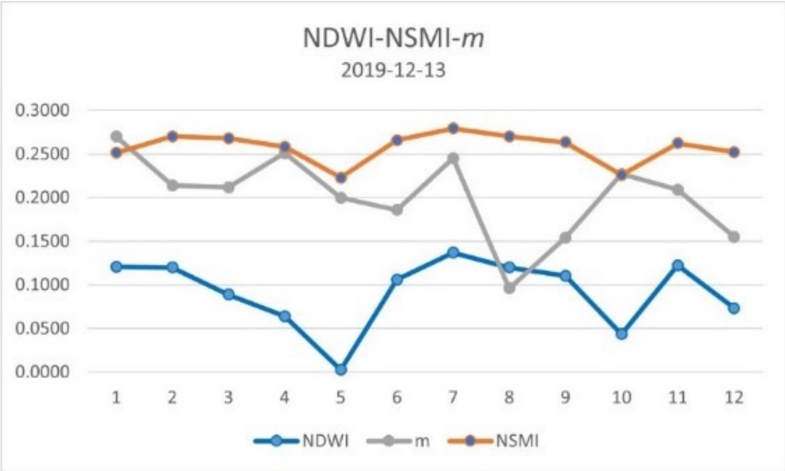

Figure 10: Comparison Trend of Measured Soil Moisture *m* with NDWI, and NSMI for the case of Dec. 13, 2019

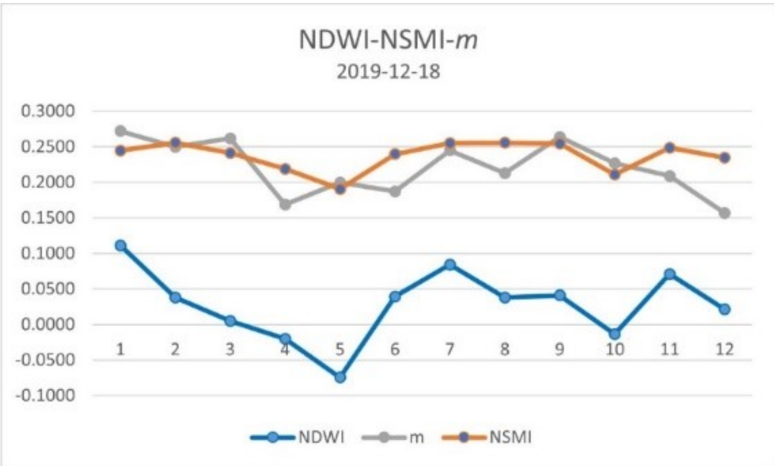

Figure 11: Comparison Trend of Measured Soil Moisture *m* with NDWI, and NSMI for the case of Dec. 18, 2019

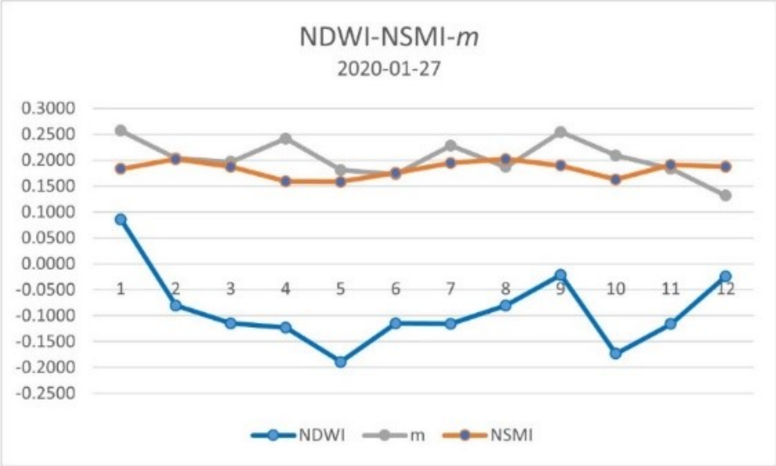

Figure 12: Comparison Trend of Measured Soil Moisture *m* with NDWI, and NSMI for the case of Jan. 27, 2020

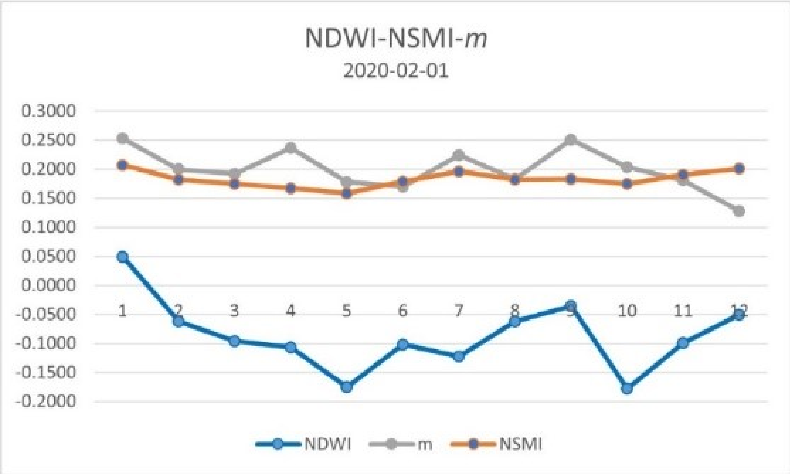

Figure 13: Comparison Trend of Measured Soil Moisture *m* with NDWI, and NSMI for the case of Feb. 01, 2020

We calculated the R^2 and p-value of the linear regression correlation between the *m* and remote sensing indices values for each sensor. For NDWI, the result is shown in Table 4 and Figure 14; and for NSMI, the result is shown in Table 5. and Figure 15. In these Figures, we have illustrated the 13 sensors as sequential numbers for simplicity.

5.2.2 Linear regression correlation between ***measured soil moisture m*** *and NSMI*

For the correlation between *m* and NDWI, the sensors No. 01A, 01B, 13A and 13B have very high $R^2 \geq 0.6$ (0.6637 – 0.87) and low p-value (0.01-0.04 < 0.05), while the sensors No.07B, 19A, 16A and 04B have high $R^2 > 0.6$ and $R^2 < 0.7$ (0.61 – 0.67) and low p-value (0.02-0.03 < 0.05). The remained sensors have low $R^2 < 0.5$ and high p-values (p-value > 0.05), which are not significant. For the correlation between *m* and NSMI, the sensors No. 01B, 13A, 13B, 19A and 04B have very high $R^2 \geq 0.7$ and $R^2 < 0.7$ (0.71 – 0.94) and low p-value (0.0003-0.01 < 0.05), while the sensors No. 01A, 07B and 16A have high $R^2 > 0.6$ and $R^2 < 0.7$ (0.66 – 0.69) and low p-value (0.01-0.02 < 0.05). The remained sensors have low $R^2 < 0.5$ and high p-values (p-value > 0.05), which are not significant. We have found here in the relationship between the value *m* of some sensor and the remote sensing indice value have a very high correlation. These sensors are No. 01A, 01B, 13A and 13B for NDWI (R^2 = 0.7951 - 0.8787) as shown in Table 5. Similarly, for the case between *m* and NSMI are the sensors No. 01B, 13A, 13B, 19A, and 04B (R^2 = 0.7183 - 0.9408).

Table 4: The R^2 and p-value of the linear regression between the *m* and NDWI value

Sensor ID	R^2	p-value
01A	0.8689	0.0022
01B	0.7951	0.0070
13A	0.8787	0.0018
10A	0.2891	0.2132
07A	0.3128	0.1918
04A	0.3921	0.1325
13B	0.8326	0.0042
07B	0.6719	0.0240
19A	0.6851	0.0215
16A	0.6140	0.0371
04B	0.6668	0.0250
25A	0.0152	0.7925
22A	0.0317	0.7025

Table 5: The R^2 and p-value of the linear regression between the *m* and NSMI value

Sensor ID	R^2	p-value
01A	0.6637	0.0256
01B	0.9099	0.0009
13A	0.9408	0.0003
10A	0.2070	0.3050
07A	0.4339	0.1076
04A	0.4723	0.0880
13B	0.7748	0.0089
07B	0.6964	0.0195
19A	0.7183	0.0160
16A	0.6944	0.0199
04B	0.7955	0.0250
25A	0.0001	0.9844
22A	0.0125	0.8114

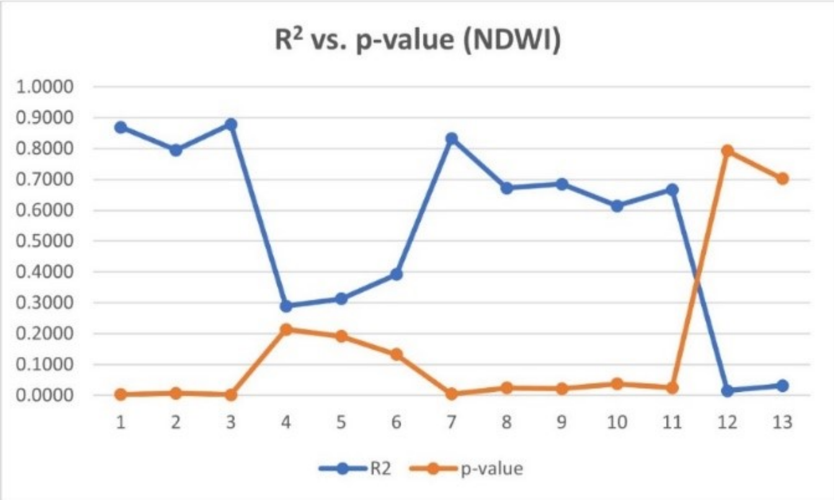

Figure 14: R2 and p-value of the correlation between m and NDWI for each sensor for in observation dates

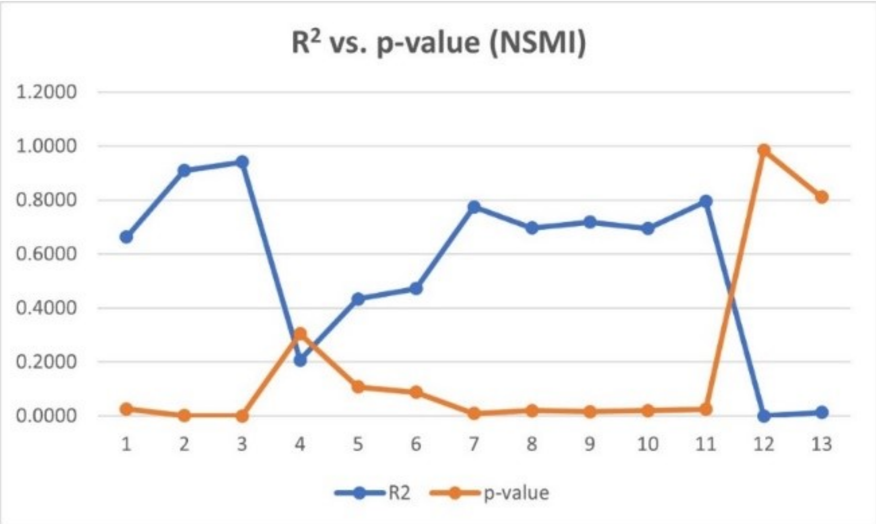

Figure 15: R^2 and p-value of the correlation between *m* and NSMI for each sensor for in observation dates

5.2.3 Sensors grouping by very high, high and low correlation between m and NDWI and NSMI

Apart of that, we have found the sensors with good correlation value between *m* and the indices. These are the sensors 07B, 19A, 16A and 04B for the case of *m* and NDWI (R^2 = 0.6140 - 0.6851) and 01A, 07B and 16A for the case of *m* and NSMI (R^2 = 0.6637 - 0.6964). The other remained sensors have R^2 lower than 0.5, which is not significant. These sensors are No. 10A, 07A, 04A, 25A, and 22A for the case between *m* and NDWI (R^2 = 0.0152 - 0.3921) and between *m* and NSMI, the sensors are 10A, 07A, 04A, 25A, and 22A (R^2 = 0.0125 - 0.4723). According to the above analysis, we have sensors in 3 groups by their R^2 values as 1) very high, 2) high and 3) low, illustrated in Google Earth map with placemarks in round shape highlighted in dark green (very high R^2), light green (high R^2), and yellow (low R^2) as shown in Figure 16. From the first group of sensors, if we select sensors 01B and 13A to group together as listed in Table 6, we obtained very high correlation value (R^2 = 0.715) between *m* value and NDWI (Figure 17), also very high correlation value (R^2 = 0.7825) for the case between *m* and NSMI (Figure 18). This shows us that these two sensors give very high correlation. Similarly, the combination of sensors 01A, 01B, and 13A (Table 7) gives very high correlation (R^2 = 0.8038) between *m* value and NDWI (Figure 19).

Figure 16: 3 groups of sensors classified by their R^2 values

Table 6: The normalised soil moisture *m* and its corresponding NDWI and NSMI values of sensors 01B and 13A

Date	ID	*m*	NDWI	NSMI
Nov. 08, 2019	01B	0.2790	0.1661	0.2884
Dec. 03, 2019	01B	0.2350	0.0416	0.2107
Dec. 08, 2019	01B	0.2280	0.0502	0.2226
Dec. 13, 2019	01B	0.2270	0.0436	0.2262
Dec. 18, 2019	01B	0.2270	-0.0137	0.2112
Jan. 27, 2020	01B	0.2090	-0.1733	0.1627
Feb. 01, 2020	01B	0.2040	-0.1778	0.1749
Nov. 08, 2019	13A	0.2570	0.1738	0.2927
Dec. 03, 2019	13A	0.2090	0.0223	0.2194
Dec. 08, 2019	13A	0.2000	-0.0006	0.1960
Dec. 13, 2019	13A	0.2000	0.0029	0.2229
Dec. 18, 2019	13A	0.2000	-0.0743	0.1906
Jan. 27, 2020	13A	0.1810	-0.1889	0.1586
Feb. 01, 2020	13A	0.1780	-0.1752	0.1583

Table 7: List of selected sensors of high correlation between *m* and NDWI

Date	ID	*m*	NDWI	NSMI
Nov. 08, 2019	01A	0.3060	0.2216	0.2672
Dec. 03, 2019	01A	0.2780	0.1597	0.2400
Dec. 08, 2019	01A	0.2710	0.1643	0.2391
Dec. 13, 2019	01A	0.2700	0.1208	0.2514
Dec. 18, 2019	01A	0.2720	0.1115	0.2445
Jan. 27, 2020	01A	0.2570	0.0861	0.1834
Feb. 01, 2020	01A	0.2530	0.0496	0.2072
Nov. 08, 2019	01B	0.2790	0.1661	0.2884
Dec. 03, 2019	01B	0.2350	0.0416	0.2107
Dec. 08, 2019	01B	0.2280	0.0502	0.2226
Dec. 13, 2019	01B	0.2270	0.0436	0.2262
Dec. 18, 2019	01B	0.2270	-0.0137	0.2112
Jan. 27, 2020	01B	0.2090	-0.1733	0.1627
Feb. 01, 2020	01B	0.2040	-0.1778	0.1749
Nov. 08, 2019	13A	0.2570	0.1738	0.2927
Dec. 03, 2019	13A	0.2090	0.0223	0.2194
Dec. 08, 2019	13A	0.2000	-0.0006	0.1960
Dec. 13, 2019	13A	0.2000	0.0029	0.2229
Dec. 18, 2019	13A	0.2000	-0.0743	0.1906
Jan. 27, 2020	13A	0.1810	-0.1889	0.1586
Feb. 01, 2020	13A	0.1780	-0.1752	0.1583
Nov. 08, 2019	13B	0.2250	0.1757	0.2782
Dec. 03, 2019	13B	0.1680	0.0941	0.2517
Dec. 08, 2019	13B	0.1600	0.1014	0.2379
Dec. 13, 2019	13B	0.1550	0.0732	0.2524
Dec. 18, 2019	13B	0.1570	0.0214	0.2348
Jan. 27, 2020	13B	0.1320	-0.0241	0.1879
Feb. 01, 2020	13B	0.1280	-0.0503	0.2016

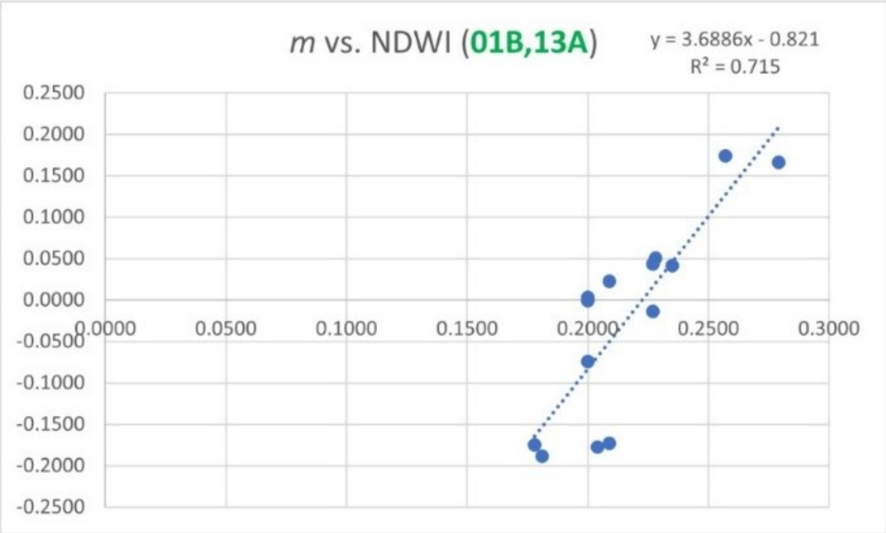

Figure 17: Correlation between *m* and NDWI for sensors 01B and 13A

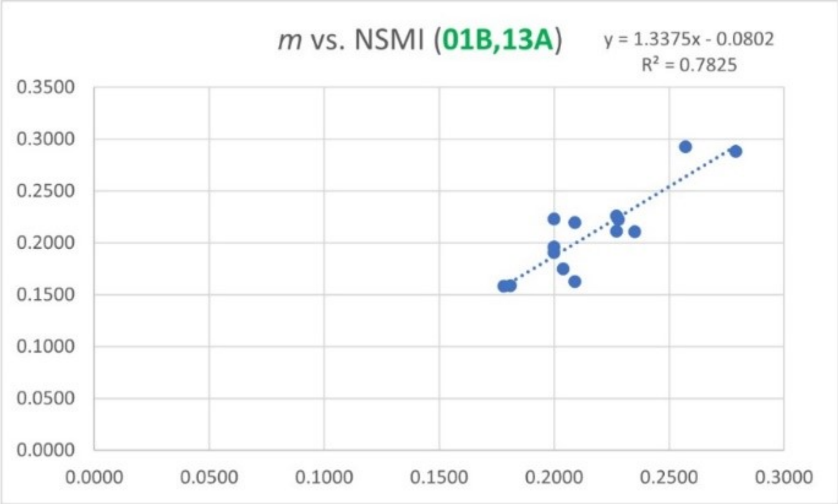

Figure 18:Correlation between *m* and NSMI for the group sensors 01B and 13A

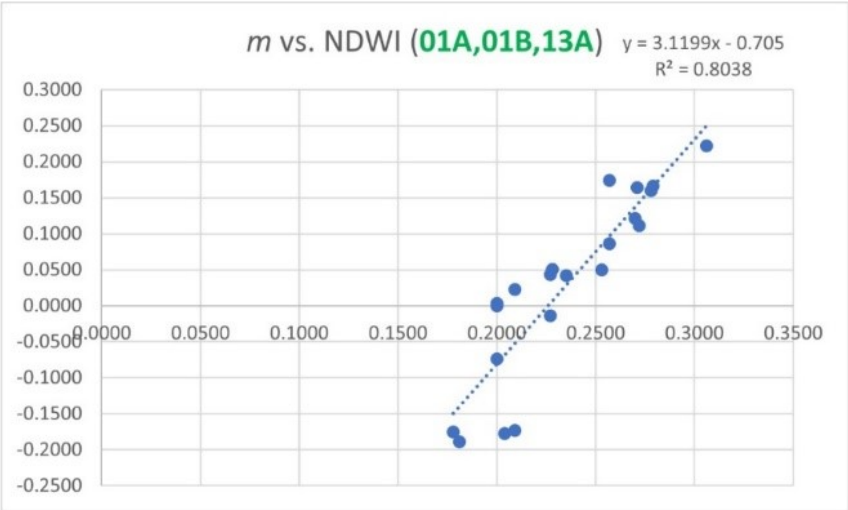

Figure 19: Correlation between *m* and NDWI for the group of sensors 01A, 01B and 13A

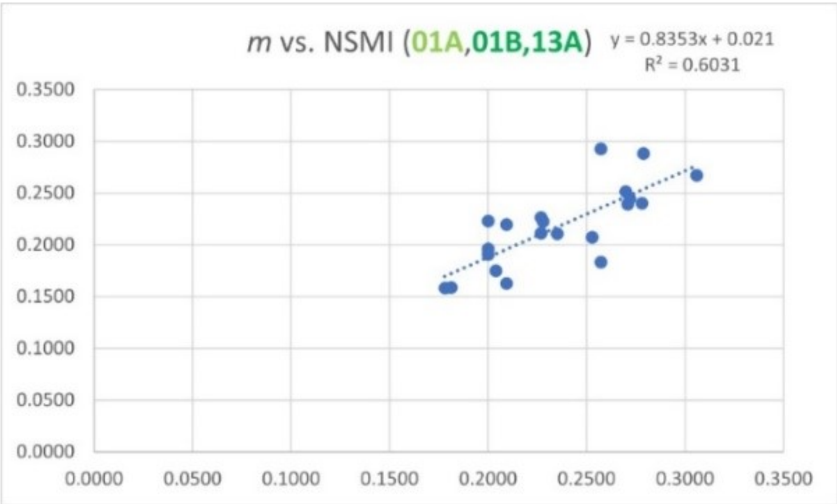

Figure 20: Correlation between m and NSMI for the group of sensors 01A, 01B and 13A

However, for the case of the correlation between *m* and NSMI for these sensors, we obtained a not very high correlation (R^2 = 0.6031) as shown in Figure 20. This shows that the group of these three sensors give very high correlation between their *m* value and NDWI, but not very high with NSMI. Also, if we group the sensors 01B, 13A, and 13B together (Table 8), we obtained a very low correlation value R^2 = 0.1184 for the case between *m* value and NDWI (Figure 21) and R^2 = 0.0590 for the case between *m* and NSMI (Figure 22). This shows that these three sensors form a combination of ground sensors that give a very low correlation. Finally, if we group all sensors 01A, 01B, 13A, and 13B together (Table 7), we obtained a low correlation value R^2 = 0.3288 (Figure 23) for the case between *m* value and NDWI, and R^2 = 0.1788 for the case of the correlation between *m* and NSMI (Figure 24). This shows that, when we added sensor No. 13B to the group of the three sensors, it causes a low correlation for the case between *m* value and NDWI. According to the analysis above, the group of the sensors 01B and 13A gives very high correlation value of R^2 for both relationships between *m* and NDWI (R^2=0.7150) and between *m* and NSMI (R^2=0.7825). When we added the sensor 01A to this group, the correlation value become much higher for the case between *m* value and NDWI (R^2 = 0.8038). For the case between *m* value and NSMI, R^2 value reduced from 0.7825 to 0.6031, however, it is still good correlation. If we added the sensor 13B to this group as the 4th sensor, the R^2 value between *m* and NDWI, as well as between *m* and NSMI, become low as 0.3288 and 0.1788, respectively.

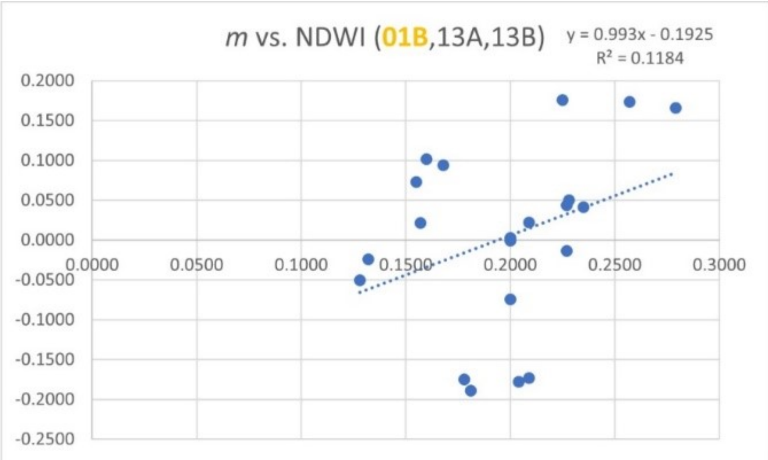

Figure 21: Correlation between *m* and NDWI for the group of sensors 01B, 13A, and 13B

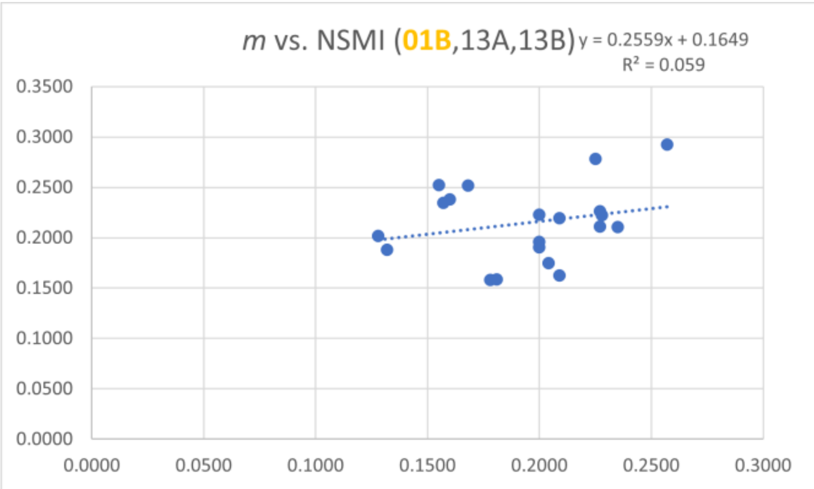

Figure 22: Correlation between *m* and NSMI for the group of sensors 01B, 13A, and 13B

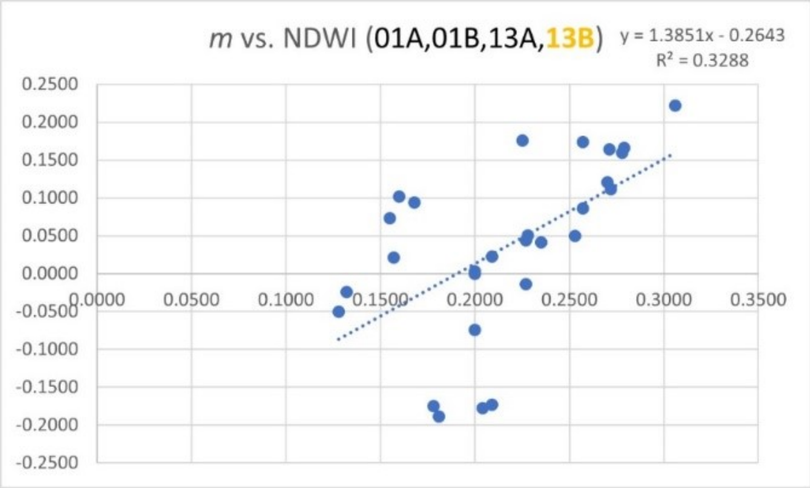

Figure 23: Correlation between *m* and NDWI for sensors 01A, 01B, 13A, and 13B

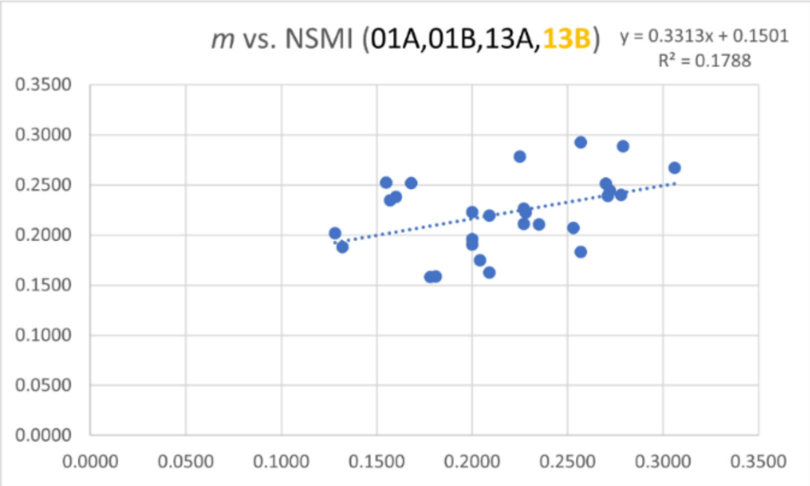

Figure 24: Correlation between *m* and NSMI for the group of sensors 01A, 01B, 13A, and 13B

Lastly, if we remove the sensor 01A from this group and remain only 01B, 13A, and 13B, the R^2 value between *m* value and NDWI, as well as between *m* value and NSMI, become very low as 0.1184 and 0.0590, respectively. Therefore, based on this result, it shows that sensor 13B causes the R^2 value to be very low, regardless sensor 13B is from the first group of sensors of very high and high R^2 values. The summary of the R^2 value related to these sensor groups is shown in Table 8. In Table 9, the correlation between *m* value and NDWI for the sensor of 01B and 13A maintain good value (R^2 = 0.7150). When sensor 01A is added, R^2 is increased to 0.8038 as very high correlation, unlike the case between *m* and NSMI, R^2 is reduced to 0.6031. After adding sensor 13B to the group of the sensor 01A, 01B and 13A, R^2 between *m* and NDWI is reduced to 0.3288, and for the case between *m* and NSMI, R^2 is reduced to 0.1788.

The R^2 value becomes also low for the correlation between *m* and NDWI (R^2 = 0.1184), similarly for the correlation between *m* and NSMI (R^2 = 0.0590), after removing the sensor 01A from this group to have only the sensor 01B, 13A, and 13B. This summary shows that NDWI is more suitable than NSMI to work on soil moisture estimation, also investigated the reason that causes different R^2 value for the correlation between *m* and NDWI, and between *m* and NSMI. According to the spatial distribution of the sensors as seen in the Google Earth image taken on Dec. 20, 2019 (Figure 16), the sensors were buried in a depth of 10 cm along with the space between the mango trees with large crowns. We assume these large crowns could be obstacle to block the satellite sensor could not detect the ground surface clearly where the soil moisture sensors are located.

Table 8: Combination of selected sensors generate highest and lowest R^2

Sensor No.				*m* vs. NDWI	*m* vs. NSMI
01A	01B	13A	13B		
				0.7150	0.7825
				0.8038	0.6031
				0.3288	0.1788
				0.1184	0.0590

Table 9: NDVI values of the sensors in the observation dates

Date	01A	01B	04A	04B	07A	07B	10A
Nov. 08, 2019	0.6801	0.6936	0.6814	0.6984	0.6853	0.7129	0.6952
Dec. 03, 2019	0.5068	0.4537	0.6329	0.5922	0.6104	0.7035	0.5359
Dec. 08, 2019	0.4962	0.4920	0.6055	0.5853	0.5591	0.6719	0.5039
Dec. 13, 2019	0.4686	0.3626	0.6167	0.5293	0.6252	0.6477	0.5716
Dec. 18, 2019	0.4377	0.3975	0.6035	0.5526	0.6084	0.6791	0.5376
Jan. 27, 2020	0.4530	0.3619	0.4757	0.4328	0.4325	0.4895	0.4162
Feb. 01, 2020	0.4228	0.3008	0.4199	0.3885	0.3787	0.4003	0.3680

Table 10: NDVI values of the sensors in the observation dates (continued)

Date	13A	13B	16A	19A	22A	25A	Min.
Nov. 08, 2019	0.6919	0.6827	0.7080	0.7129	0.6814	0.6902	0.6801
Dec. 03, 2019	0.4488	0.5259	0.6293	0.7035	0.6329	0.6622	0.4488
Dec. 08, 2019	0.4065	0.4764	0.6232	0.6719	0.6055	0.6055	0.4065
Dec. 13, 2019	0.4466	0.4927	0.5623	0.6477	0.6167	0.6341	0.3626
Dec. 18, 2019	0.4212	0.4714	0.5866	0.6791	0.6035	0.6570	0.3975
Jan. 27, 2020	0.3340	0.4465	0.4569	0.4895	0.4757	0.5353	0.3340
Feb. 01, 2020	0.2977	0.4002	0.4018	0.4003	0.4199	0.4803	0.2977

For example, for sensor 13B and others which give very low R^2 value between *m* values and NDWI and NSMI as well. To prove this assumption, we have generated a time-series of NDVI images of the study area for all observation dates, from Nov. 08, 2019 to Feb. 01, 2020 to analyse the vegetation cover at the image pixel location of the sensors, as shown in Table 9 and its continued Table 10. The idea is the lower the NDVI value, the lesser vegetation cover, which means the ground surface is exposed as an open space, and thus, the satellite sensor could detect the reflected energy from the ground, so the soil moisture index NSMI can be generated more accurate as there is less obstacle from the mango tree crows or other surround vegetation to cover the ground surface where the soil moisture sensors are located. On the contrary, the higher the NDVI value, the more vegetation cover, which means the ground surface is blocked and thus, the satellite sensor could not efficiently detect the reflected energy from the ground, so the soil moisture index NSMI can be generated less accurate as there is more obstacle from the mango tree crows or other surround vegetation to cover the ground surface where the soil moisture sensors are located. Based on this idea, we need to investigate the minimum NDVI value among these sensors in the observation period. At first, we allocate the minimum NDVI value of all sensors for each observation date, which the result is shown in the pre-last column of the Tables 9 and 10. Next, we investigate the minimum NDVI value of each sensor's location for all observation dates. The result shows that, for the first case of the investigation, the minimum NDVI value is found which is 0.2977, and belong to the sensor 13A. The other nearest minimum NDVI value to this is the minimum NDVI value of sensor 13A(0.2977) and 01B (0.3008), respectively, which ranges from 0.29 to 0.30.

Therefore, the remained minimum NDVI value of each sensor ranges from 0.36 to 0.42 as well as the minimum NDVI value of all sensors for each observation date ranges from 0.3340 to 0.6801, and it is larger than the minimum NDVI value of 0.2977 of sensor 13A. Therefore, the minimum NDVI values found here are 0.2977 and 0.3008, and are belong to the sensor 13A and 01B, respectively. This shows that, the NDVI pixels of these two sensors are related to the sparse vegetation cover as the NDVI is less than 0.3. Consequently, *m* values of the sensors 13A and 01B located at the less vegetation cover pixels have a very high correlation with NDWI and NSMI, than other sensors in the image pixels of NDVI larger than 0.3.

6. Conclusions

After studying the relationship between soil moisture measured by the ground sensor and the remote sensing indices which are related to the soil moisture (NSMI), vegetation-related (NDVI), and vegetation water-content (NDWI) in the study area, we concluded that, among the remote sensing indices, the result shows that the measure soil moisture *m* have a similar trend with NDWI. The correlation between *m* and NDWI and NSMI in the observation period is high, comparing with other indices. The spatial analysis shows that applying the correlation of these remote sensing indices NDWI and NSMI; we can see that the density of the vegetation influences the correlation between *m* and these indices. In the location of sparse vegetation density, the correlation value is higher than in the location of dense vegetation density. Finally, it is concluded that NDWI and NSMI are suitable remote sensing indices for estimating the soil moisture data from satellite imagery in the land cover where NDVI is less than 0.3.

As the results have been observed, some of the sensor's data display a very good, good, and low or poor correlation with their corresponding remote sensing indices which are NDWI and NSMI. According to this finding, this gives us the idea to explore more and analyze more deeply to find out why some sensors provide such different correlation levels? That is becoming a very challenging question to find out the reason behind this. Therefore, at the end of the in-deep analysis for a different group of sensors and different remote sensing indices, the result shows that the higher NDVI at the sensor location, the less the correlation value. That tells us there are some 'things' behaves as an 'obstacle' to disturb or influence the correlation values. In our case, the surrounding vegetation cover blocks the reflecting energy from the soil where the sensor locates to the satellite sensor.

Acknowledgements

We would like to thanks to the Agricultural Research Development Agency (ARDA) of Thailand for their sponsorship on financial support under Grant PRP6205030620 for this research project. The authors are grateful to the Copernicus program of the European Space Agency (ESA) for accessing the Sentinel-2 data used in this research.

References

Alexandridis, T. K., Cherif, I., Bilas, G., Waldenio G. A., Hartanto, I. M., Jan van Andel, S. and Araujo A., 2016, Spatial and Temporal Distribution of Soil Moisture at the Catchment Scale Using Remotely-Sensed Energy Fluxes. Water, Vol. 8(32), doi:10.3390/w8010032.

Ahmad, A., Zhang, Y. and Nichols. S., 2011, Review and Evaluation of Remote Sensing Methods for Soil-Moisture Estimation. *SPIE Reviews*, Vol.2(1), DOI: 10.1117/1.3534910.

Babaeian, E., Sidike, P., Newcomb, M. S., Maimaitijiang, M., White, S. A., Demieville, J., Ward, R. W., Sadeghi, M., LeBauer, D. S., Jones, S. B., Sagan, V. and Tuller, M., 2019, A New Optical Remote Sensing Technique for High-Resolution Mapping of Soil Moisture. *Frontiers in Big Data*, Vol.2(37), 1-6, doi: 10.3389/fdata.2019.00037.

Carmelo, A., Pilar, L., Rosa, M. B. and Tarquis, A. M., 2019, Correlation between Vegetation Index and Soil Moisture Index Using Sentinel-2. *Conference: XIV Jornadas de Investigación en la Zona No Saturada del SueloAt: Madrid*. 1-5.

Filion, R., Bernier, M., Paniconi, C., Chokmani, K., Melis, M., Soddu, A., Talazac, M. and Lafortune, F. X., 2016, Remote Sensing for Mapping Soil Moisture and Drainage Potential in Semi-Arid Regions: Applications to the Campidano Plain of Sardinia, Italy. *Science of the Total Environment* 2016, Vol. 543, 862-876. https://doi.org/10.1016/j.scitotenv.2015.07.068.

Gao, B., 1996, NDWI-A Normalized Difference Water Index for Remote Sensing of Vegetation Liquid Water from Space. *Remote Sensing of Environment*, Vol. 58(3), 257-266. https://doi.org/10.1016/S0034-4257(96)00067-3.

Klemas, V., Finkl, C.W. and Kabbara, N., 2014, Remote Sensing of Soil Moisture: An Overview in Relation to Coastal Soils. *Journal of Coastal Research*, Vol. 30(4), 685–696, DOI: 10.2112/JCOASTRES-D-13-00072.1.

Park, S., Park, S., Im, J., Rhee, J., Shin, J. and Park, J. D., 2017, Downscaling GLDAS Soil Moisture Data in East Asia through Fusion of Multi-Sensors by Optimizing Modified Regression Trees. *Water*, Vol. 9*,* doi:10.3390/w9050332.

Petropoulos, G. P., Ireland, G. and B. Barrett, 2015, Surface Soil Moisture Retrievals from Remote Sensing: Current Status, Products and Future Trends. *Physics and Chemistry of the Earth*, Vol. 83, 36-56. https://doi.org/10.1016-/j.pce.2015.02.009.

Ray, R. L., Fares, A., He, Y. and Temimi, M., 2017, Evaluation and Inter-Comparison of Satellite Soil Moisture Products Using in Situ Observations over Texas, U.S., *Water*, Vol. 9*,* doi:10.3390/w9060372.

Torres-Rua, A. F., Ticlavilca, A. M., Bachour, R. and McKee, M., 2016, Estimation of Surface Soil Moisture in Irrigated Lands by Assimilation of Landsat Vegetation Indices, Surface Energy Balance Products, and Relevance Vector Machines. *Water*, Vol. 8(4), doi:10.3390/w-8040167.

Wikipedia, 2021, Sentinel-2, viewed on 17 August 2019,https://en.wikipedia.org/wiki/Sentinel-2.